European Journal of Mechanics / A Solids 104 (2024) 105218

Contents lists available at ScienceDirect

European Journal of Mechanics / A Solids

journal homepage: www.elsevier.com/locate/ejmsol

Full length article

Buckling and post-buckling analysis of double-layer magnetoelectric nano-plate strips considering piezo-flexoelectric and piezo-flexomagnetic effects

Hamed Momeni-Khabisi, Masoud Tahani *

Department of Mechanical Engineering, Ferdowsi University of Mashhad, Mashhad, Iran

ARTICLE INFO

Keywords:
Buckling and post-buckling
Closed-form solution
Magnetoelectric plate strip
Size-dependent theories
Piezo-flexoelectric
Piezo-flexomagnetic

ABSTRACT

In the present work, closed-form solutions for the linear and nonlinear stability of the magnetoelectric nanoplate strips consisting of piezo-flexoelectric and piezo-flexomagnetic layers are presented. In the framework of the nonlocal strain gradient and first-order shear deformation theories, magneto-electro-mechanical responses are obtained for simply supported and clamped end conditions. Excellent agreements are observed between the obtained results and the existing literature. The effect of several parameters on critical buckling load and post-buckling path is investigated. Our outcomes reveal that the post-buckling load-carrying capacity increases considerably in the case of a double-layer ME nano-plate strip compared to a single-layer (piezo-flexoelectric and piezo-flexomagnetic) with the same thickness and length. Further, the post-buckling deformation decreases with a decrease in initial electric voltage and an increase in initial magnetic potential. The closed-form solutions and numerical results of this work are useful for future analyses and the design of such nanostructures.

1. Introduction

Micro- and nano-electromechanical systems (MEMs/NEMs) have been considered for various applications including sensors, actuators, and energy harvesters on very small scales in the last decade. Currently, these systems are generally used in various industries such as aerospace, information technology, telecommunications, and robotics. Therefore, electromechanical coupling plays a key role in the application of MEMs and NEMs (Zubko et al., 2013; Zhang et al., 2019; Moradi-Dastjerdi et al., 2019).

One of the most famous electromechanical couplings is the piezoelectric property, which reflects the response of an electric field to a uniform strain. Similar to piezoelectrics, piezomagnetic materials can release strain energy in the form of a magnetic field due to mechanical strain (Eliseev et al., 2009; Kabychenkov and Lisovskii, 2019; Ebrahimi and Karimiasl, 2018).

Many studies have shown that the presence of non-uniform strain, or in other words strain gradient, can induce an electric field in the dielectric material. Such a coupling is called the flexoelectric effect. Unlike piezoelectricity, the flexoelectric effect exists in all materials even with centrosymmetric crystal structures (Kundalwal et al., 2020; Gupta et al., 2022). The flexoelectric effect is responsible for the size-dependent electroelastic responses of piezoelectric nanomaterials, therefore, it should be considered to describe the electromechanical coupling in these materials. Similar to flexoelectricity, the bending of some materials due to the presence of flexomagnetic creates a magnetic field. The magnetic polarization produced by the non-uniform strain distribution is called the flexomagnetic effect (Majdoub et al., 2008; Yang and Li, 2019; Zhang et al., 2019). The flexo-electric/magnetic effect has a great effect on the performance of structures at the micro and nano scales, and ignoring this effect can cause numerous inaccuracies in the calculations and evaluation of these structures (Kundalwal and Gupta, 2022).

Among the various methods of supplying electrical energy from various environmental energy sources, the use of magnetic energy and its conversion into electricity has been given much attention (Ryu et al., 2015). Magnetic energy can be absorbed through electromagnetic devices made of coils and permanent magnets (Yuan et al., 2015) as well as magnetoelectric (ME) composites (Kambale et al., 2014; Li et al., 2007; Zhang et al., 2009). ME composite materials are an important class of smart materials that combine piezoelectric and piezomagnetic phases.

Most of the articles on ME composites are related to multilayers and particles due to the potential applications of these structures in transducers (Zhang et al., 2020), magnetic field sensors, actuators,

* Corresponding author.
E-mail address: mtahani@um.ac.ir (M. Tahani).

https://doi.org/10.1016/j.euromechsol.2023.105218
Received 5 October 2023; Received in revised form 28 November 2023; Accepted 22 December 2023
Available online 27 December 2023

Nomenclature

$(N_{xx}, M_{xx}, Q_x, N_{xxz})$	Stress resultants
(u_0, w_0)	Displacements of a point on the mid-plane
η_{ijk}	Strain gradient components
l	Strain gradient parameter
$\mathcal{H}$	Enthalpy density
$\mu = (e_0 a)^2$	Nonlocal parameter
μ_{3113}	Coefficient of flexoeffect
ν	Poisson's ratio
Φ	Electric potential
ϕ	Rotation of a transverse normal about the y-axis
ψ	Scalar magnetic potential
Ψ_1	External magnetic potential
σ_{ij}	Stress components
τ_{xxz}	Higher-order stress
ε_0	Permittivity of vacuum
ε_{ij}	Strain components
a_{33}	Components of magnetic permeability
A_{55}	Extensional stiffness coefficient
B_z	Magnetic induction vector
C_{55}	Shear modulus
d_{31}	Coefficient of piezomagnetic
e_{31}	Coefficient of piezoelectric
E_z	Electric field
g_{113113}	Component of the strain gradient elasticity tensor
h	Thickness of a plate strip
H_z	Component of magnetic field vector across the thickness
K_s	Shear correction factor
L	Length of nano-plate strip along the x-axis
P_z	Electric polarization
Q_{ij}	Coefficients of plane stress reduced stiffness
u	Axial component of the displacement field
V_1	External electric voltage
V_{zz}	Higher-order electric field
w	Transverse component of displacement field

magnetic energy harvesters (Ge et al., 2018; Zhang et al., 2021), high-speed memories (Bibes and Barthélémy, 2008), data storage devices, miniature antennas (Cheng et al., 2018), and for powering devices and stimulating cells, and tissues by applying external magnetic fields (Ribeiro et al., 2016; Shi et al., 2021).

To the best of the authors' knowledge, no research has yet been reported on the buckling of magnetoelectric nanostructures by simultaneously considering the effects of flexoelectric and flexomagnetic properties. Therefore, in this section, we will have an overview of some of the related studies.

Using the finite element method, Kumaravel et al. (2007) investigated the linear thermal buckling and free vibration behavior of the layered and multiphase magneto-electro-elastic beam with clamped boundary conditions. Li (2014) studied the buckling and free vibrations of magneto-electro-elastic nanoplates based on the nonlocal Mindlin theory. They ignored the in-plane electric and magnetic fields. Ansari and Gholami (2016) used nonlinear nonlocal first-order shear deformation theory (FSDT) to analyze the post-buckling of magneto-electro-thermo-elastic nanobeams. Ebrahimi and Barati (2016b) studied the buckling of functionally graded magneto-electro-elastic nanoplates located in an elastic Pasternak medium based on the modified nonlocal four-variable plate theory. They also evaluated the buckling behavior of curved magneto-electro-elastic nanobeams based on the nonlocal elasticity theory (Ebrahimi and Barati, 2016a).

Ansari and Gholami (2017) evaluated the buckling and post-buckling of magneto-electro-elastic nanoplates under thermal loading through the nonlocal form of the Mindlin plate theory. Buckling analysis of piezo-magnetoelectric nanoplates in a hygrothermal environment, electric voltage, and external magnetic potential was investigated by Malikan and Nguyen (2018) and the effect of different parameters on the critical buckling load was studied. Żur et al. (2020) investigated the free vibrations and buckling of functionally graded magneto-electro-elastic nanoplates based on the nonlocal modified sinusoidal higher-order shear deformation theory. The forced oscillation equation of rectangular sandwich plates at the micro and nano-scale using a modified dynamic version of Hamilton's principle including electric and magnetic parts was established and the closed-form solution for simply supported boundary conditions was obtained using Navier's method.

Modeling of thermal post-buckling behavior of magneto-electro-elastic multilayer beams with the Timoshenko theory and considering von-Kármán nonlinear strains was done by Zhang et al. (2021). The first research in the field of magnetoelectric nanostructures consisting of a piezo-flexomagnetic (PFM) layer and a piezo-flexoelectric (PFE) layer was done by Shi et al. (2021). They obtained the governing equations and boundary conditions in tensorial form for a nanobeam considering an Euler–Bernoulli beam theory. They investigated the magnetoelectric response of double-layer nanobeams and presented a closed-form expression for the magnetoelectric voltage, demonstrating the necessity of considering the flexo-electric/magnetic effects in the modeling of ME nanocomposites.

Liang et al. (2015) investigated the surface effects and flexoelectricity on buckling and vibrations of piezoelectric nanowires based on the Euler–Bernoulli theory. They showed that the effects of surface piezoelectricity and flexoelectricity play an important role in determining the critical buckling voltage. Electromechanical and size-dependent buckling behavior of PFE nanobeams based on nonlocal theories and surface elasticity were studied by Ebrahimi and Barati (2018). They assumed that these nanobeams are in contact with a two-parameter elastic support (consisting of an infinite linear spring and a shear layer). They investigated the effect of nonlocal parameter, surface effects, geometrical parameters, elastic support, and boundary conditions on the buckling of flexoelectric nanobeams.

Ebrahimi and Karimiasl (2018) studied surface and flexoelectric effects on the buckling of piezoelectric sandwich nanobeam with the Winkler–Pasternak elastic support. Their results showed that especially in small thicknesses, the nonlocal parameter reduces the critical load and flexoelectricity increases the buckling load. Ebnali Samani and Tadi Beni (2018) investigated the mechanical and thermal buckling of flexoelectric nanobeam based on the Timoshenko model and considering the geometric nonlinear effects. Their results showed that at the nano-scale, the flexoelectric effect strongly affects the piezoelectricity, and flexoelectric materials can be used as alternatives to make various sensors and actuators.

Barati and Zenkour (2019) analyzed the thermal buckling of piezoelectric nanobeams with geometrical imperfection by considering surface and flexoelectric effects. They investigated the effects of surface tension, flexoelectricity, applied electric voltage, geometrical imperfection, foundation parameters, and boundary conditions on the post-buckling load of piezoelectric nanobeams. Their results showed that both surface effects and flexoelectricity have a significant influence on the post-buckling behavior of the system, and only flexoelectricity makes a major difference between their model and previous research on conventional piezoelectric nanobeams. Esmaeili and Tadi Beni (2019) investigated the buckling and free vibrations of a functionally graded flexoelectric nanobeam based on the Euler–Bernoulli

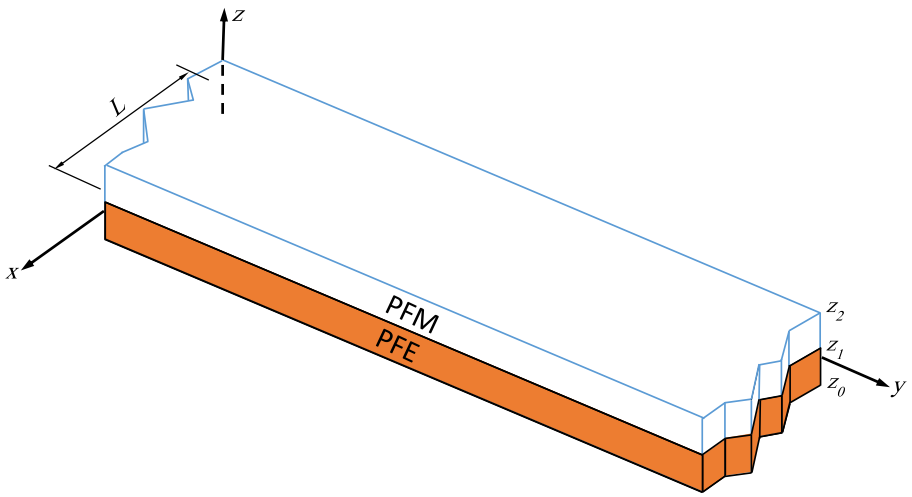

Fig. 1. Schematic of a magnetoelectric nano-plate strip with PFE layer at the bottom and PFM layer at the top supported with SS and CC end conditions.

theory. They found that increasing the flexoelectric factor increases the critical buckling load and natural frequency.

Amir et al. (2020) performed the buckling analysis of nanocomposite sandwich plates with piezoelectric layers based on the FSDT and they solved the governing equations analytically. In this research, the critical buckling voltage was calculated by considering the effect of flexoelectric and it was shown that flexoelectric has a significant effect on the critical buckling voltage. In addition, it was found that the thickness of the flexoelectric layers and the aspect ratio of the sandwich plate plays an important role in the changes in the critical buckling load. Increasing the thickness of flexoelectric face sheets and the aspect ratio reduces the critical buckling load and vice versa. Zhao et al. (2022) analyzed bending, free vibrations, and buckling of flexoelectric nanobeam based on the Euler–Bernoulli beam theory. The nanobeam was functionally graded along the axis and the strain gradient theory was used to apply the size effect. The governing equations were obtained based on Hamilton's principle and solved with generalized differential quadrature method, and the effect of flexoelectricity, strain gradient, and heterogeneous distribution of materials on mechanical behavior was investigated. Duc et al. (2022) investigated the influence of geometric and material parameters on free vibrations and static buckling of flexoelectric nanoplates with variable thickness. Their results showed a great effect of flexoelectric on the buckling behavior and the shape of the vibration modes, also the working performance is increased. By changing different models of thickness change, they showed that the effect of flexoelectric significantly changes the mechanical response of the plate.

Malikan et al. (2020b) analyzed the post-buckling of PFM nanobeams with various boundary conditions using nonlocal strain gradient (NSG) theory. They used Euler–Bernoulli theory and nonlinear von-Kármán strains to obtain the mathematical model. One of their results was that the flexomagnetic effect is more pronounced in nanobeams whose boundary conditions have fewer degrees of freedom. Investigating the effect of different asymmetric and axially symmetric porosity distributions on the stability of nanobeams under the effects of piezomagnetic and converse flexomagnetic (CFM) through NSG theory and taking into account infinitesimal strains and Euler–Bernoulli theory was done by Malikan et al. (2020a). They obtained a closed-form relation for critical buckling load by the Navier method.

The biaxial buckling of the PFM nanoplates was investigated by using the classical plate theory, infinitesimally small strains, and NSG theory in simply supported (SS) boundary conditions and clamped support by Malikan and Eremeyev (2021a). Effects of magnetic field, aspect ratio, flexomagnetic, and nonlocal parameter on critical load were discussed. They found that the flexomagnetic value can be affected by the aspect ratio of the plate. Malikan and Eremeyev (2021b) investigated the effect of shear deformations on the CFM response of piezomagnetic nanobeams. They obtained the governing equations by considering linear strains and using the Timoshenko and NSG theories and used the Galerkin method to solve these equations and estimate the critical buckling load in the case of SS boundary conditions.

Zhang et al. (2022a) investigated the static bending, free vibrations, and buckling of bent flexomagnetic nanobeams with SS end conditions. Based on the Hamilton principle, strain gradient theory, and Timoshenko beam model, they obtained the governing equations and boundary conditions and then solved the governing differential equations using the Navier method. They discussed the effects of opening angle, aspect ratio, and length scale parameter on bending deformation, free vibrations, and buckling. Also, Zhang et al. (2022b) investigated static bending, free vibrations, and buckling of flexomagnetic nanoplates with SS end conditions. They obtained the governing equations and boundary conditions using Hamilton's principle based on the strain gradient theory and classical plate theory. Then the governing differential equations were solved using the Navier method. They discussed the effects of flexomagnetic, aspect ratio, and length scale parameter on static bending deformation, free vibrations, and stability analysis of nanoplates.

Using the FSD theory, Momeni-Khabisi and Tahani (2022) analyzed the mechanical buckling and post-buckling behavior of nano-plate strips considering the effect of flexomagnetic and investigated the effect of important parameters on the stability of such nanostructures. They used the NSG theory to model the size effects and derived the governing equations using the principle of minimum total potential energy and solved them based on the weighted residual Galerkin method for SS boundary conditions. In another study, Momeni-Khabisi and Tahani (2023) investigated thermal buckling and post-buckling of shear deformable nano-plate strips with piezomagnetic and flexomagnetic effects. They obtained the closed-form solutions for thermal buckling and thermal post-buckling path in the case of imperfect nano-plate strips with SS end conditions in a hygrothermal environment. They considered uniform, linear, and non-linear distributions across the thickness for temperature rise and studied the effect of small-scale parameters, slenderness ratio of the plate, initial rise of the mid-plane, temperature distribution, and magnetic potential on thermal stability.

The literature review, which focuses on stability analysis, PFE, PFM, and ME problems, shows that there is no published work on the stability of magnetoelectric structures considering simultaneously the PFE and PFM effects. Due to the importance and application of the flexo-electric/magnetic effect in nanostructures, the necessity for extensive mechanical analyses in magnetoelectric nanostructures to predict their behavior or improve their performance is clear. To facilitate the design and manufacturing processes, the present study

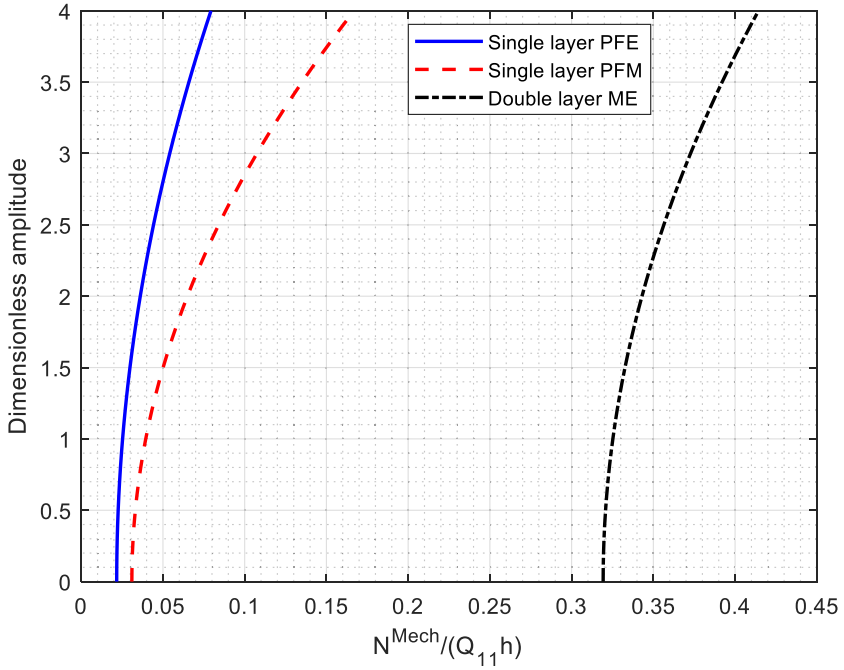

Fig. 2. Dimensionless amplitude versus non-dimensional post-buckling loads.

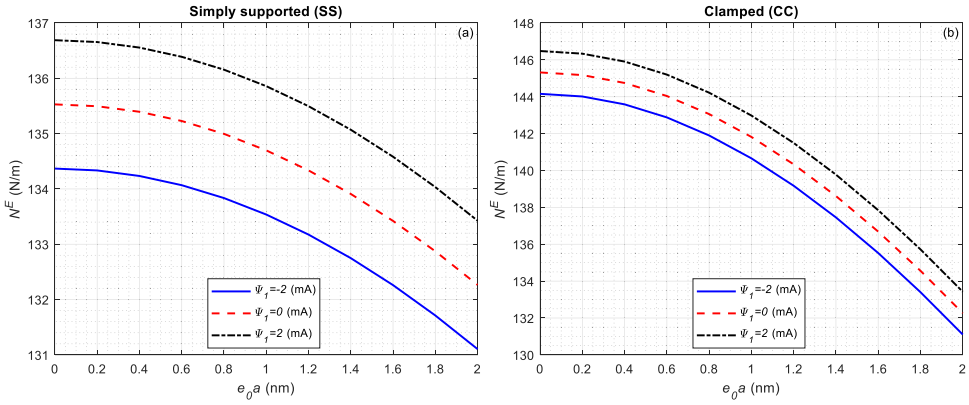

Fig. 3. The electric resultant versus the nonlocal parameter for different scalar magnetic potentials. (a) Simply-supported and (b) clamped end conditions.

deals with the effect of flexo-electric/magnetic on the buckling and post-buckling loads of double-layer ME nano-plate strips consisting of a PFE layer ($BaTiO_3$) at the bottom and a PFM layer ($CoFe_2O_4$) at the top. The size-dependent governing equations are derived based on the principle of minimum total potential energy and considering von-Kármán's nonlinear strains, nonlocal strain gradient theory, and first-order shear deformation theory. Closed-form solutions are obtained for simply supported and clamped end conditions and the numerical results are validated with existing literature. Then, the influence of scalar magnetic potential, electric voltage, nonlocal parameter, strain gradient parameter, length-to-thickness ratio, dimensionless amplitude, and flexo-electric/magnetic effects on linear and nonlinear buckling loads are investigated. The presented closed-form solutions and numerical results may be useful for future analyses and the design of such nanostructures.

2. Modeling of the problem

The ME coupling causes the piezomagnetic phase to deform due to magnetostriction when a magnetic field is applied. The strain created in the piezomagnetic phase passes through the piezoelectric phase due to the mechanical contact between the two phases and leads to polarization in the piezoelectric phase. Similarly, by applying an electric field, strain is created in the piezoelectric phase and mechanically transferred to the piezomagnetic phase, and its deformation leads to magnetization in the piezomagnetic phase (Pandey et al., 2019). In order to develop efficient ME structures at the nanoscale and fully exploit these advanced nanostructures, it is essential to understand their mechanical responses, which are expected to be different from macroscopic mechanisms.

In this section, the buckling and post-buckling behavior of a nano-plate strip consisting of piezo-flexoelectric and piezo-flexomagnetic double-layer are modeled (Fig. 1). The lower layer ($z_0 < z < z_1$) is made of $BaTiO_3$ and the upper layer ($z_1 < z < z_2$) is made of $CoFe_2O_4$. Nano-plate strip is located in the x-y plane and its total thickness along the z-axis is equal to h. Its length is equal to L along the x-axis and its width along the y-axis is equal to b ($b \gg L$). It should be noted that the plate strip is a particular case of the rectangular plate that is longer in one direction than the other. In this case, the displacement components can only be assumed to be a function of the smaller direction (i.e., x) and all derivatives with respect to the larger dimension (i.e., y) are zero (Reddy, 2006). Simply supported and

clamped–clamped (CC) boundary conditions on both sides along the x-axis have been studied. Nano-plate strip is exposed to the electric voltage V_1 between surfaces $z = z_0$ and $z = z_1$ as well as the magnetic potential Ψ_1 between surfaces $z = z_1$ and $z = z_2$. Note that $z_1 = z_0$ and $z_1 = z_2$ correspond to the single-layer PFM and single-layer PFE, respectively.

To consider the effects of transverse shear deformation, the first-order shear deformation theory is used. On the framework of the FSDT, the components of the displacement field are expressed as:

$$\begin{aligned} u(x,z) &= u_0(x) + z\phi(x) \\ w(x,z) &= w_0(x) \end{aligned} \tag{1}$$

The nonlinear strain–displacement relations based on the von-Kármán hypothesis can be written as:

$$\begin{aligned} &\varepsilon_{xx} = \varepsilon^0_{xx} + z\varepsilon^1_{xx} \\ &\gamma_{xz} = \gamma^0_{xz} \\ &\varepsilon_{yy} = \varepsilon_{zz} = \gamma_{xy} = \gamma_{yz} = 0 \\ &\eta_{xxz} = \frac{\mathrm{d}\phi}{\mathrm{d}x} \\ &\eta_{yyz} = \eta_{xyz} = 0 \end{aligned} \tag{2}$$

where

$$\begin{aligned} \varepsilon^0_{xx} &= \frac{\mathrm{d}u_0}{\mathrm{d}x} + \frac{1}{2}\left(\frac{\mathrm{d}w_0}{\mathrm{d}x}\right)^2 \\ \gamma^0_{xz} &= \phi + \frac{\mathrm{d}w_0}{\mathrm{d}x} \\ \varepsilon^1_{xx} &= \frac{\mathrm{d}\phi}{\mathrm{d}x} \end{aligned} \tag{3}$$

The relationship between the component of magnetic field vector across the thickness and the scalar magnetic potential is stated as below:

$$H_z = -\frac{\partial \psi}{\partial z} \tag{4}$$

The constitutive equations for the stress components (σ_{ij}), higher-order stress components (τ_{ijk}), electric field (E_i), higher-order electric field (V_{ij}), and magnetic induction vector (B_i) can be written as (Zhao et al., 2022; Shi et al., 2021):
in case of PFE layer

$$\begin{aligned} &{}^p\sigma_{xx} = {}^pQ_{11}\varepsilon_{xx} + {}^pQ_{12}\varepsilon_{yy} + e_{31}P_z - {}^p\mu_{3113}\frac{\partial P_z}{\partial z} \\ &{}^p\sigma_{xz} = {}^pC_{55}\gamma_{xz} \\ &{}^p\tau_{xxz} = {}^p\mu_{3113}P_z + 2({}^p\alpha_2 + {}^p\alpha_4)\eta_{xxz} \\ &E_z = {}^pa_{33}P_z + e_{31}\varepsilon_{xx} + {}^p\mu_{3113}\eta_{xxz} \\ &V_{zz} = {}^pb_{33}\frac{\partial P_z}{\partial z} - {}^p\mu_{3113}\varepsilon_{xx} \end{aligned} \tag{5}$$

and in case of PFM layer:

$$\begin{aligned} &{}^m\sigma_{xx} = {}^mQ_{11}\varepsilon_{xx} + {}^mQ_{12}\varepsilon_{yy} - d_{31}H_z \\ &{}^m\sigma_{xz} = {}^mC_{55}\gamma_{xz} \\ &{}^m\tau_{xxz} = {}^mg_{113113}\eta_{xxz} - {}^m\mu_{3113}H_z \\ &B_z = {}^ma_{33}H_z + d_{31}\varepsilon_{xx} + {}^m\mu_{3113}\eta_{xxz} \end{aligned} \tag{6}$$

where superscripts p and m are used for PFE and PFM layers, respectively. The parameters ${}^pb_{33}$, ${}^p\alpha_2$, and ${}^p\alpha_4$ are related to the material length scale parameters (Zhao et al., 2022). Q_{ij} are the plane stress reduced stiffness coefficients and g_{113113} is the component of the strain gradient elasticity tensor. The definition of Q_{ij} and g_{113113} components are given in Appendix A. The first variation of the enthalpy density can be written as follows (Zhao et al., 2022; Shi et al., 2021; Sidhardh and Ray, 2018):

$$\begin{aligned} \delta\mathcal{H} = \int_A\int_{z_0}^{z_2} \Big(&\sigma_{xx}\delta\varepsilon_{xx} + \sigma_{xz}\delta\gamma_{xz} + \tau_{xxz}\delta\eta_{xxz} + E_z\delta P_z + V_{zz}\delta\frac{\partial P_z}{\partial z} \\ &- B_z\delta H_z + \frac{\partial \Phi}{\partial z}\delta P_z + P_z\delta\frac{\partial \Phi}{\partial z} - \varepsilon_0\frac{\partial \Phi}{\partial z}\delta\frac{\partial \Phi}{\partial z}\Big)\,\mathrm{d}z\mathrm{d}A \end{aligned} \tag{7}$$

By combining Eqs. (2)–(7) and using the divergence theorem, one can obtain:

$$\begin{aligned} \delta\mathcal{H} = &+\left[\int_0^b \left(N_{xx}\delta u_0 + N_{xx}\frac{\mathrm{d}w_0}{\mathrm{d}x}\delta w_0 + M_{xx}\delta\phi + Q_x\delta w_0 \right.\right. \\ &\left.\left. + N_{xxz}\delta\phi\right)\mathrm{d}y\right]_{x=0}^{x=L} \\ &+\left[\int_A B_z\delta\psi\,\mathrm{d}A\right]_{z=z_1}^{z=z_2} + \left[\int_A V_{zz}\delta P_z\,\mathrm{d}A\right]_{z=z_0}^{z=z_1} \\ &+\left[\int_A \left(P_z - \varepsilon_0\frac{\partial \Phi}{\partial z}\right)\delta\Phi\,\mathrm{d}A\right]_{z=z_0}^{z=z_1} \\ &\int_A\left[-\frac{\mathrm{d}N_{xx}}{\mathrm{d}x}\delta u_0 - \frac{\mathrm{d}}{\mathrm{d}x}\left(N_{xx}\frac{\mathrm{d}w_0}{\mathrm{d}x}\right)\delta w_0 - \frac{\mathrm{d}M_{xx}}{\mathrm{d}x}\delta\phi + Q_x\delta\phi - \frac{\mathrm{d}Q_x}{\mathrm{d}x}\delta w_0\right. \\ &\left.-\frac{\mathrm{d}N_{xxz}}{\mathrm{d}x}\delta\phi\right]\mathrm{d}A \\ &-\int_A\int_{z_1}^{z_2}\frac{\partial B_z}{\partial z}\delta\psi\,\mathrm{d}z\mathrm{d}A + \int_A\int_{z_0}^{z_1}\left(E_z + \frac{\partial \Phi}{\partial z}\right)\delta P_z\,\mathrm{d}z\mathrm{d}A \\ &-\int_A\int_{z_0}^{z_1}\frac{\partial V_{zz}}{\partial z}\delta P_z\,\mathrm{d}z\mathrm{d}A \\ &-\int_A\int_{z_0}^{z_1}\left(\frac{\partial P_z}{\partial z} - \varepsilon_0\frac{\partial^2 \Phi}{\partial z^2}\right)\delta\Phi\,\mathrm{d}z\mathrm{d}A \end{aligned} \tag{8}$$

where the stress resultants $\left(N_{xx}, M_{xx}, Q_x, N_{xxz}\right)$ are defined in Appendix B.

The work done by the external force N^0_{xx} can be obtained as follows:

$$\begin{aligned} \delta W_E &= \delta\left[-\frac{1}{2}\int_0^b\int_0^L N^0_{xx}\left(\frac{\mathrm{d}w_0}{\mathrm{d}x}\right)^2\mathrm{d}x\mathrm{d}y\right] \\ &= -\int_0^b\int_0^L N^0_{xx}\frac{\mathrm{d}w_0}{\mathrm{d}x}\frac{\mathrm{d}\delta w_0}{\mathrm{d}x}\mathrm{d}x\mathrm{d}y \\ &= -\left[\int_0^b N^0_{xx}\frac{\mathrm{d}w_0}{\mathrm{d}x}\delta w_0\mathrm{d}y\right]_{x=0}^{x=L} + \int_0^b\int_0^L\frac{\mathrm{d}}{\mathrm{d}x}\left(N^0_{xx}\frac{\mathrm{d}w_0}{\mathrm{d}x}\right)\delta w_0\mathrm{d}x\mathrm{d}y \\ &= -\left[\int_0^b N^0_{xx}\frac{\mathrm{d}w_0}{\mathrm{d}x}\delta w_0\mathrm{d}y\right]_{x=0}^{x=L} + \int_A N^0_{xx}\frac{\mathrm{d}^2w_0}{\mathrm{d}x^2}\delta w_0\mathrm{d}A \end{aligned} \tag{9}$$

By applying the principle of minimum total potential energy ($\delta\mathcal{H} - \delta W_E = 0$), the equilibrium, electrical, and magnetic equations are obtained as:

$$\delta u_0 : \quad \frac{\mathrm{d}N_{xx}}{\mathrm{d}x} = 0 \tag{10}$$

$$\delta w_0 : \quad \frac{\mathrm{d}}{\mathrm{d}x}\left(N_{xx}\frac{\mathrm{d}w_0}{\mathrm{d}x}\right) + \frac{\mathrm{d}Q_x}{\mathrm{d}x} + N^0_{xx}\frac{\mathrm{d}^2w_0}{\mathrm{d}x^2} = 0 \tag{11}$$

$$\delta\phi : \quad \frac{\mathrm{d}M_{xx}}{\mathrm{d}x} + \frac{\mathrm{d}N_{xxz}}{\mathrm{d}x} - Q_x = 0 \tag{12}$$

$$\delta\Phi : \quad \frac{\partial P_z}{\partial z} - \varepsilon_0\frac{\partial^2 \Phi}{\partial z^2} = 0 \tag{13}$$

$$\delta P_z : \quad E_z + \frac{\partial \Phi}{\partial z} - \frac{\partial V_{zz}}{\partial z} = 0 \tag{14}$$

$$\delta\psi : \quad \frac{\partial B_z}{\partial z} = 0 \tag{15}$$

The boundary conditions involve the specification of

$$\begin{aligned} &\delta u_0 = 0 \quad \text{or} \quad N_{xx} = 0 && \text{at } x = 0, L \\ &\delta w_0 = 0 \quad \text{or} \quad N_{xx}\frac{\mathrm{d}w_0}{\mathrm{d}x} + Q_x + N^0_{xx}\frac{\mathrm{d}w_0}{\mathrm{d}x} = 0 && \text{at } x = 0, L \\ &\delta\phi = 0 \quad \text{or} \quad M_{xx} + N_{xxz} = 0 && \text{at } x = 0, L \\ &\delta\Phi = 0 \quad \text{or} \quad P_z - \varepsilon_0\frac{\partial \Phi}{\partial z} = 0 && \text{at } z = z_0, z_1 \\ &\delta P_z = 0 \quad \text{or} \quad V_{zz} = 0 && \text{at } z = z_0, z_1 \\ &\delta\psi = 0 \quad \text{or} \quad B_z = 0 && \text{at } z = z_1, z_2 \end{aligned} \tag{16}$$

By substituting Eqs. (2) and (3) into E_z and V_{zz} of Eq. (5) and using Eq. (13) we obtain:

$$E_z = {}^{p}a_{33}\left(\varepsilon_0\frac{\partial \boldsymbol{\Phi}}{\partial z} - c_1\right) + e_{31}\left[\frac{\mathrm{d}u_0}{\mathrm{d}x} + z\frac{\mathrm{d}\phi}{\mathrm{d}x} + \frac{1}{2}\left(\frac{\mathrm{d}w_0}{\mathrm{d}x}\right)^2\right] + {}^{p}\mu_{3113}\frac{\mathrm{d}\phi}{\mathrm{d}x} \tag{17}$$

$$V_{zz} = {}^{p}b_{33}\varepsilon_0\frac{\partial^2 \boldsymbol{\Phi}}{\partial z^2} - {}^{p}\mu_{3113}\left[\frac{\mathrm{d}u_0}{\mathrm{d}x} + z\frac{\mathrm{d}\phi}{\mathrm{d}x} + \frac{1}{2}\left(\frac{\mathrm{d}w_0}{\mathrm{d}x}\right)^2\right] \tag{18}$$

Using Eqs. (17), (18), and (14), we have:

$$\begin{aligned}&{}^{p}a_{33}\left(\varepsilon_0\frac{\partial \boldsymbol{\Phi}}{\partial z} - c_1\right) + e_{31}\left[\frac{\mathrm{d}u_0}{\mathrm{d}x} + z\frac{\mathrm{d}\phi}{\mathrm{d}x} + \frac{1}{2}\left(\frac{\mathrm{d}w_0}{\mathrm{d}x}\right)^2\right] + {}^{p}\mu_{3113}\frac{\mathrm{d}\phi}{\mathrm{d}x} + \frac{\partial \boldsymbol{\Phi}}{\partial z}\\ &- {}^{p}b_{33}\varepsilon_0\frac{\partial^3 \boldsymbol{\Phi}}{\partial z^3} + {}^{p}\mu_{3113}\frac{\mathrm{d}\phi}{\mathrm{d}x} = 0\end{aligned} \tag{19}$$

By integrating the above equation and solving the resulting second-order equation, we obtain:

$$\begin{aligned}\boldsymbol{\Phi} = {}&c_3 e^{{}^{p}\lambda z} + c_4 e^{-{}^{p}\lambda z} - \frac{e_{31}}{2\left(1+{}^{p}a_{33}\varepsilon_0\right)}\frac{\mathrm{d}\phi}{\mathrm{d}x}z^2 - \frac{e_{31}{}^{p}b_{33}\varepsilon_0}{\left(1+{}^{p}a_{33}\varepsilon_0\right)^2}\frac{\mathrm{d}\phi}{\mathrm{d}x}\\ &+ \frac{c_2}{\left(1+{}^{p}a_{33}\varepsilon_0\right)}\\ &+ \frac{\left[-2{}^{p}\mu_{3113}\frac{\mathrm{d}\phi}{\mathrm{d}x} - \frac{1}{2}e_{31}\left(\frac{\mathrm{d}w_0}{\mathrm{d}x}\right)^2 - e_{31}\frac{\mathrm{d}u_0}{\mathrm{d}x} + c_1{}^{p}a_{33}\right]z}{\left(1+{}^{p}a_{33}\varepsilon_0\right)}\end{aligned} \tag{20}$$

where c_1, c_2, c_3, and c_4 are constants of integration. By substituting Eq. (20) into Eq. (18) and using the boundary conditions of the higher-order electric field (i.e., $V_{zz} = 0$ at $z = z_0$ and z_1), the constants c_3 and c_4 are obtained. Then, by substituting them into Eq. (20) and using the boundary conditions of the electric potential (i.e., $\phi = 0$ at $z = z_0$ and $\phi = V_1$ at $z = z_1$), the electric potential and, accordingly, using Eq. (13), the electric polarization and the electric polarization gradient are obtained as:

$$\begin{aligned}\boldsymbol{\Phi} = {}&m_1\frac{\mathrm{d}u_0}{\mathrm{d}x} + \left(m_2 e^{{}^{p}\lambda z} + m_3 e^{-{}^{p}\lambda z} + m_4 z + m_5\frac{z^2}{2} + m_6\right)\frac{\mathrm{d}\phi}{\mathrm{d}x}\\ &+ \frac{1}{2}m_1\left(\frac{\mathrm{d}w_0}{\mathrm{d}x}\right)^2 + V_1\frac{z}{(z_1-z_0)} - \frac{z_0}{(z_1-z_0)}V_1\end{aligned} \tag{21}$$

$$P_z = m_7\frac{\mathrm{d}u_0}{\mathrm{d}x} + K_1\frac{\mathrm{d}\phi}{\mathrm{d}x} + \frac{1}{2}m_7\left(\frac{\mathrm{d}w_0}{\mathrm{d}x}\right)^2 - \frac{V_1}{{}^{p}a_{33}(z_1-z_0)} \tag{22}$$

$$\frac{\partial P_z}{\partial z} = m_9\frac{\mathrm{d}u_0}{\mathrm{d}x} + K_2\frac{\mathrm{d}\phi}{\mathrm{d}x} + \frac{1}{2}m_9\left(\frac{\mathrm{d}w_0}{\mathrm{d}x}\right)^2 \tag{23}$$

where m_1 to m_9 and K_1 and K_2 are given in Appendix A. It is worth mentioning that similar relationships have been reported by Zhao et al. (2022).

The scalar magnetic potential $\psi(x, z)$ can be obtained using Eqs. (2)–(4), (6), and (15) with the corresponding magnetic boundary conditions at $z = z_1$ and $z = z_2$ as follows:

$$\psi(x,z) = \frac{d_{31}}{2^{m}a_{33}}\left[z^2 - z(z_2+z_1) + z_1 z_2\right]\frac{\mathrm{d}\phi}{\mathrm{d}x} + \frac{\Psi_1}{z_2-z_1}(z-z_1) \tag{24}$$

By combining Eqs. (2)–(4) and (21)–(23) with Eqs. (5) and (6) and replacing the results into Eq. (B.1), the stress resultants are obtained in terms of displacement components as given in Appendix B.

Substituting Eq. (B.2) into Eq. (10) and integrating leads to the following equation:

$$D_1\frac{\mathrm{d}u_0}{\mathrm{d}x} + D_2\frac{\mathrm{d}\phi}{\mathrm{d}x} + \frac{1}{2}D_1\left(\frac{\mathrm{d}w_0}{\mathrm{d}x}\right)^2 + D_3 = c \tag{25}$$

where c is a constant related to the axial tensile force due to the mid-plane stretching. To remove the axial displacement u_0, integrating Eq. (25) and then employing the classical and non-classical boundary conditions of Eq. (16) the following equation is obtained (She et al., 2017; Li and Hu, 2017):

$$D_1\frac{\mathrm{d}u_0}{\mathrm{d}x} + D_2\frac{\mathrm{d}\phi}{\mathrm{d}x} + \frac{1}{2}D_1\left(\frac{\mathrm{d}w_0}{\mathrm{d}x}\right)^2 = \frac{D_1}{2L}\int_0^L\left(\frac{\mathrm{d}w_0}{\mathrm{d}x}\right)^2\mathrm{d}x \tag{26}$$

By substituting Eq. (26) into Eqs. (B.2)–(B.5) and then applying the NSG theory (Lim et al., 2015) one can obtain:

$$\left(1-\mu\nabla^2\right)N_{xx} = \left(1-l^2\nabla^2\right)\left[\frac{D_1}{2L}\int_0^L\left(\frac{\mathrm{d}w}{\mathrm{d}x}\right)^2\mathrm{d}x + D_3\right] \tag{27}$$

$$\begin{aligned}\left(1-\mu\nabla^2\right)M_{xx} = {}&\left(1-l^2\nabla^2\right)\left[\frac{D_4}{2L}\int_0^L\left(\frac{\mathrm{d}w}{\mathrm{d}x}\right)^2\mathrm{d}x + \frac{D_1D_5 - D_2D_4}{D_1}\frac{\mathrm{d}\phi}{\mathrm{d}x}\right.\\ &\left.+D_6\right]\end{aligned} \tag{28}$$

$$\begin{aligned}\left(1-\mu\nabla^2\right)N_{xxz} = {}&\left(1-l^2\nabla^2\right)\left[\frac{D_7}{2L}\int_0^L\left(\frac{\mathrm{d}w}{\mathrm{d}x}\right)^2\mathrm{d}x + \frac{D_1D_8 - D_2D_7}{D_1}\frac{\mathrm{d}\phi}{\mathrm{d}x}\right.\\ &\left.+D_9\right]\end{aligned} \tag{29}$$

$$\left(1-\mu\nabla^2\right)Q_x = \left(1-l^2\nabla^2\right)\left[K_sA_{55}\left(\frac{\mathrm{d}w}{\mathrm{d}x} + \phi\right)\right] \tag{30}$$

By differentiation with respect to x from Eqs. (11) and (12) and inserting the results into Eqs. (28)–(30), we obtain:

$$M_{xx} + N_{xxz} - \mu\frac{\mathrm{d}Q_x}{\mathrm{d}x} = \left(1-l^2\nabla^2\right)\left[\frac{D_1+D_4}{2L}\int_0^L\left(\frac{\mathrm{d}w}{\mathrm{d}x}\right)^2\mathrm{d}x + \overline{D}\frac{\mathrm{d}\phi}{\mathrm{d}x} + D_9\right] \tag{31}$$

$$Q_x + \mu\left(N_{xx} + N^0_{xx}\right)\frac{\mathrm{d}^3w}{\mathrm{d}x^3} = \left(1-l^2\nabla^2\right)\left[K_sA_{55}\left(\frac{\mathrm{d}w}{\mathrm{d}x} + \phi\right)\right] \tag{32}$$

Substituting Eqs. (31) and (32) into Eqs. (11) and (12) the governing differential equations are obtained as below:

$$\begin{aligned}&K_sA_{55}\left[\frac{\mathrm{d}^2w}{\mathrm{d}x^2} + \frac{\mathrm{d}\phi}{\mathrm{d}x} - l^2\left(\frac{\mathrm{d}^4w}{\mathrm{d}x^4} + \frac{\mathrm{d}^3\phi}{\mathrm{d}x^3}\right)\right] + \left[\frac{D_1}{2L}\int_0^L\left(\frac{\mathrm{d}w}{\mathrm{d}x}\right)^2\mathrm{d}x\right.\\ &\left.+D_3 + N^0_{xx}\right]\left(\frac{\mathrm{d}^2w}{\mathrm{d}x^2} - \mu\frac{\mathrm{d}^4w}{\mathrm{d}x^4}\right) = 0\end{aligned} \tag{33}$$

$$\overline{D}\left(\frac{\mathrm{d}^2\phi}{\mathrm{d}x^2} - l^2\frac{\mathrm{d}^4\phi}{\mathrm{d}x^4}\right) - K_sA_{55}\left[\frac{\mathrm{d}w}{\mathrm{d}x} + \phi - l^2\left(\frac{\mathrm{d}^3w}{\mathrm{d}x^3} + \frac{\mathrm{d}^2\phi}{\mathrm{d}x^2}\right)\right] = 0 \tag{34}$$

where the nonlocal parameter ($\mu = e_0a^2$) and the strain gradient parameter (l) are used to capture the size-dependent behavior of small-scale structures in NSG theory, and

$$\overline{D} = \frac{D_1(D_5+D_8) - D_2(D_4+D_7)}{D_1} \tag{35}$$

3. Analytical solution

The closed-form solutions of the governing equations in the case of SS and CC boundary conditions along the edges $x = 0, L$ are obtained in this section. To this aim, the following functions are considered:
in the case of SS boundary conditions:

$$w(x) = \sum_{m=1}^{\infty}\widetilde{W}\sin\left(\frac{m\pi x}{L}\right),\ \phi(x) = \sum_{m=1}^{\infty}\tilde{\phi}\cos\left(\frac{m\pi x}{L}\right) \tag{36}$$

and in the case of CC boundary conditions:

$$w(x) = \sum_{m=1}^{\infty}\widetilde{W}\sin^2\left(\frac{m\pi x}{L}\right),\ \phi(x) = \sum_{m=1}^{\infty}\tilde{\phi}\sin\left(\frac{2m\pi x}{L}\right) \tag{37}$$

where $\widetilde{W}$ and $\tilde{\phi}$ are the unknown coefficients of buckled configuration. Upon substitution of Eqs. (36) and (37) into Eqs. (33) and (34) one can obtain:
in the case of SS boundary conditions:

$$N^{Mech} = -N^0_{xx} = \frac{\overline{D}\alpha_m^2\lambda_{lm}}{A_1\lambda_{\mu m}} + \frac{D_1}{4}\alpha_m^2\widetilde{W}^2 + D_3 \tag{38}$$

and in the case of CC boundary conditions:

$$N^{Mech} = -N^0_{xx} = \frac{4\overline{D}\alpha_m^2\lambda'_{lm}}{A'_1\lambda'_{\mu m}} + \frac{D_1}{4}\alpha_m^2\widetilde{W}^2 + D_3 \tag{39}$$

Table 1
Magneto-electro-mechanical properties (Zhao et al., 2022; Malikan et al., 2021).

Properties	$CoFe_2O_4$	$BaTiO_3$
E (GPa)	286	131
ν	0.32	0.3
d_{31} (N/A m)	580.3	0
${}^{m}a_{33}$ (N/A^2)	157×10^{-6}	0
${}^{m}\mu_{3113}$ (N/A)	10^{-9}	0
e_{31} (V/m)	0	1.87×10^{8}
${}^{p}a_{33}$ (V m/C)	0	0.79×10^{8}
${}^{p}\mu_{3113}$ (V)	0	5

Table 2
Comparison of dimensionless linear buckling load of Timoshenko beams with simply supported and clamped boundary conditions.

		Present	Gunda (2014)	Gupta et al. (2009)
$\beta = 25$	SS	9.4062	9.4073	9.4062
	CC	32.9790	33.2314	32.9791
$\beta = 50$	SS	9.7495	9.7495	9.7495
	CC	37.6247	37.6292	37.6248
$\beta = 100$	SS	9.8393	9.8393	9.8393
	CC	38.9981	38.9981	38.9984
$\beta \to \infty$	SS	9.8696	9.8696	9.8696
	CC	39.4784	39.4784	39.4785

It should be noted that N^{Mech} is critical buckling load at $\widetilde{W} = 0$ and in case of $\widetilde{W} \neq 0$, N^{Mech} presents the post-buckling load, where

$$A_1 = 1 + \frac{\overline{D}\alpha_m^2}{K_s A_{55}}, \quad \alpha_m = \frac{m\pi}{L}, \quad \lambda_{lm} = 1 + l^2\alpha_m^2, \quad \lambda_{\mu m} = 1 + \mu\alpha_m^2,$$
$$A_1' = 1 + \frac{4\overline{D}\alpha_m^2}{K_s A_{55}}, \quad \lambda'_{lm} = 1 + 4l^2\alpha_m^2, \quad \lambda'_{\mu m} = 1 + 4\mu\alpha_m^2 \tag{40}$$

4. Numerical results and discussion

In this section, numerical results are presented for the first buckling mode ($m = 1$) of the magnetoelectric nano-plate strip which includes a piezo-flexoelectric layer at the bottom and a piezo-flexomagnetic layer on the top. The properties of PFE layer ($BaTiO_3$) and PFM layer ($CoFe_2O_4$) are defined in Table 1. It should be noted that the total thickness (h) is 2 nm and the thickness of each layer is $h/2$.

As stated, no research was found in the field of analyzing the mechanical or thermal stability of magnetoelectric nanostructures by simultaneously considering the piezo-flexoelectric and piezo-flexomagnetic effects. Therefore, to ensure validation, some numerical results of special cases of the present study are compared with those existing in the literature. To this end, three cases are considered. A single-layer nanostructure without PFM and PFE effects, a single-layer nanostructure with PFE effects, and a single-layer nanostructure with PFM effects.

First of all, the numerical results are compared with those obtained by Gunda (2014) and Gupta et al. (2009), who employed the Rayleigh–Ritz method to express the closed-form solutions for the buckling of Timoshenko beams without magnetoelectric effects. In Tables 2 and 3, the non-dimensional linear buckling load and the ratio of non-dimensional nonlinear buckling loads to non-dimensional linear buckling loads without magnetoelectric effects are presented, respectively. In these tables, β is the slenderness ratio of the beam.

Moreover, some numerical results in the case of single-layer PFE nanobeams are compared with Zhao et al. (2022). Table 4 presents the dimensionless critical buckling loads of a Timoshenko piezo-flexoelectric nanobeam.

Finally, in the case of the single-layer piezo-flexomagnetic nano-plate strip with SS end conditions and FSD theory and without thermal effect and geometrical imperfection, the buckling and post-buckling loads in Eq. (38) can be simplified to that derived by Momeni-Khabisi and Tahani (2022).

Table 3
Comparison of dimensionless post-buckling load to dimensionless buckling load ratio of simply supported and clamped Timoshenko beams.

		Present	Gunda (2014)	Gupta et al. (2009)
$\beta = 25$	SS	1.2623	1.2623	1.2623
	CC	1.0748	1.0742	1.0748
$\beta = 50$	SS	1.2531	1.2531	1.2531
	CC	1.0656	1.0656	1.0656
$\beta = 100$	SS	1.2508	1.2508	1.2508
	CC	1.0633	1.0633	1.0633
$\beta \to \infty$	SS	1.2500	1.2500	1.2500
	CC	1.0625	1.0625	1.0625

Table 4
Comparison of dimensionless linear buckling load of flexoelectric nanobeams with clamped and simply supported boundary conditions.

			$h/l = 1$	$h/l = 2$	$h/l = 10$
SS	Without FE[a]	Present	55.4216	21.2576	10.3251
		Zhao et al. (2022)	55.5946	21.3009	10.3269
	With FE	Present	53.6188	19.4165	8.1780
		Zhao et al. (2022)	53.7918	19.4598	8.1797
CC	Without FE	Present	221.6865	85.0304	41.3005
		Zhao et al. (2022)	225.1437	86.2629	41.8211
	With FE	Present	214.4751	77.6661	32.7120
		Zhao et al. (2022)	217.8427	78.8070	33.1258

[a] Flexoelectric effect.

As can be observed, there is excellent agreements between the results of the present study and those obtained by other researchers. In the following, the numerical results of buckling and post-buckling of the magnetoelectric nano-plate strips are presented considering the piezo-flexoelectric and piezo-flexomagnetic effects.

Dimensionless buckling load in terms of dimensionless amplitude is presented in Fig. 2 ($h = 2$ nm, $V_1 = -5$ V, $\Psi_1 = 2$ mA, $L/h = 20, l/h = 1, e_0a/h = 0.5$). As shown in this figure, an increase in dimensionless amplitude will increase dimensionless buckling loads. Furthermore, the dimensionless buckling loads for single-layer piezo-flexoelectric (PFE) and single-layer piezo-flexomagnetic (PFM) configurations are observed to be lower than those of double-layer magnetoelectric nano-plate strips with the same thickness. Therefore, the buckling stability of double-layer ME nano-plate strips is more than the other two cases.

Fig. 3 shows the variation of the electric resultant $N^E = V_1 e_{31}/{}^{p}a_{33}$ in terms of the nonlocal parameter e_0a for different scalar magnetic potentials Ψ_1 in both simply supported and clamped nano-plate strips ($h = 2$ nm, $L/h = 20, \widetilde{W}/h = 0$). It is concluded that the electric resultant decrease with increasing the nonlocal parameter due to decreasing the nano-plate strip stiffness. Also, increasing the applied magnetic potential leads to an increase in the electric resultant. Hence, increasing the initial applied magnetic potential will increase the stiffness of the system.

To further investigate the buckling behavior of ME nano-plate strips, the effect of external magnetic potential and electric voltage is demonstrated simultaneously in Figs. 4 and 5 ($h = 2$ nm, $L/h = 20, l/h = 0.5, e_0a/h = 0.1, \widetilde{W}/h = 0$). The initial magnetic potential has a direct effect on the critical buckling loads, while, the initial electric voltage has an inverse effect. It means an increase in applied magnetic potential and the electric voltage leads to an increase and decrease in the critical buckling loads, respectively.

Fig. 6 demonstrates the effect of small-scale parameters on dimensionless critical buckling loads ($h = 2$ nm, $V_1 = 1$ V, $\Psi_1 = 2$ mA, $L/h = 20, \widetilde{W}/h = 0$). As shown, an increase in the length scale parameter leads to an increase in buckling loads while the nonlocal parameter has an inverse effect. Also, the small-scale parameters increase or decrease the stiffness depending on the relation between them. When $e_0a > l$ and $e_0a < l$, stiffness-softening and stiffness-hardening can be

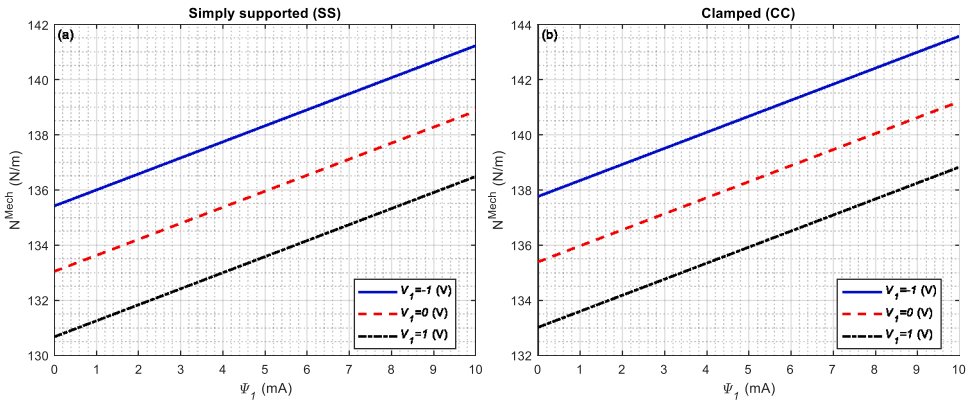

Fig. 4. Critical buckling load versus scalar magnetic potential for different electric voltages. (a) Simply-supported and (b) clamped end conditions.

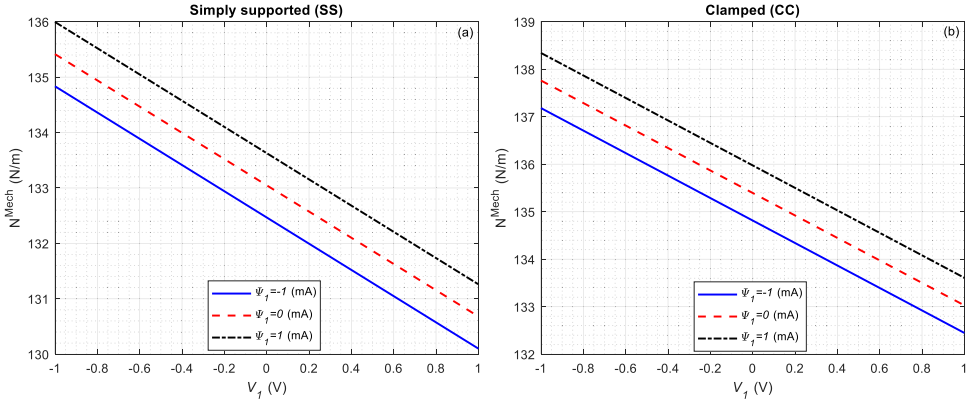

Fig. 5. Critical buckling load versus initial electric voltage for different magnetic potentials. (a) Simply-supported and (b) clamped end conditions.

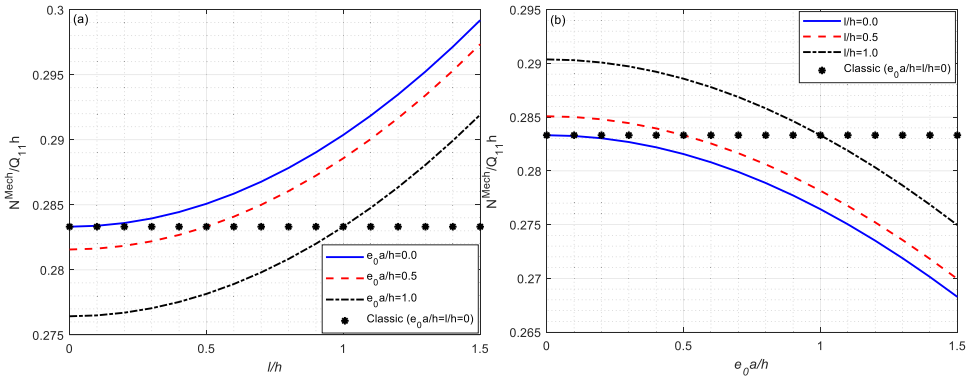

Fig. 6. Dimensionless buckling load versus (a) the ratio of length scale parameter to thickness and (b) the ratio of nonlocal parameter to thickness for different nonlocal and length scale parameters, respectively.

observed, respectively. Note that classic means without considering the small-scale parameters ($e_0 a = l = 0$).

The post-buckling path of magnetoelectric nano-plate strips subjected to different initial electric voltages is depicted in Fig. 7 for SS and CC boundary conditions ($h = 2$ nm, $\Psi_1 = 1$ mA, $L/h = 20, l/h = 2, e_0 a/h = 0.1$). The positive electric voltages lead to larger post-buckling deformations and decrease the buckling loads while the negative electric voltages have an inverse influence. Therefore, the higher positive electric voltages decrease the stability of ME nano-plate strips. From the physical standpoint, the reason is that the initial negative (positive) electric voltages generate a tensile (compressive) load and lead to a increase (decrease) in the stiffness of magnetoelectric nano-plate strips.

Fig. 8 illustrates the effect of applied magnetic potential on the post-buckling responses of ME nano-plate strips ($h = 2$ nm, $V_1 = 1$ V, $L/h = 20, l/h = 2, e_0 a/h = 0.1$). As observed, the dimensionless amplitude with applied negative magnetic potential increases and the buckling load capacity decreases since negative magnetic potential induce a compressive force and decrease the stiffness of ME nano-plate strips. In other words, a positive initial magnetic potential improves the stability of ME nano-plate strips by reducing dimensionless amplitude and increasing stiffness.

The effect of the slenderness ratio on dimensionless buckling ($\widetilde{W}/h = 0$) and post-buckling ($\widetilde{W}/h = 0.5$) loads for SS and CC boundary conditions is plotted in Fig. 9 ($h = 2$ nm, $V_1 = -1$ V, $\Psi_1 = 1$ mA, $l/h = 0.5, e_0 a/h = 0.1$). As expected, the stability of ME nano-plate strips reduces with an increase in length. Improvement of the stability

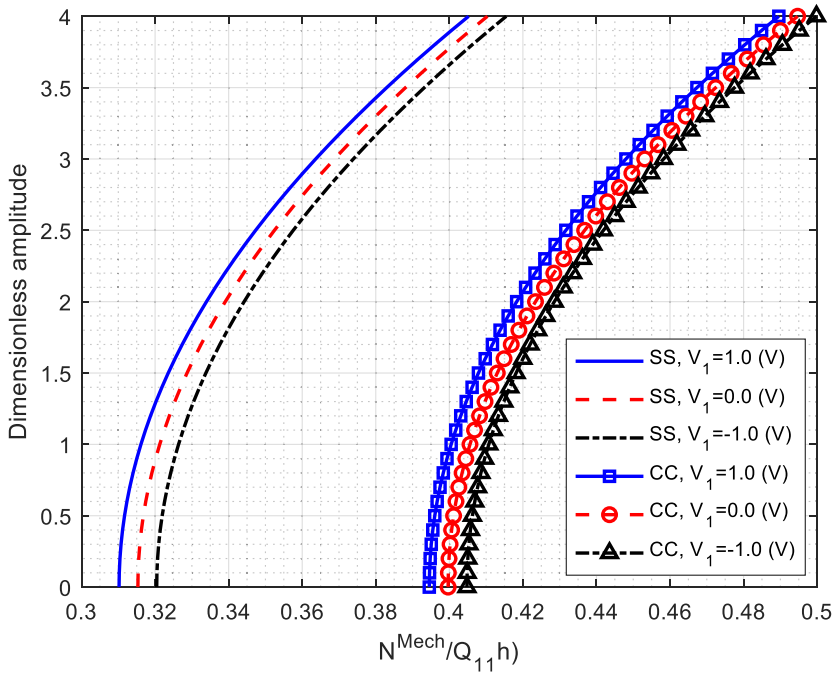

Fig. 7. Dimensionless amplitude versus dimensionless nonlinear buckling load in different electric voltages.

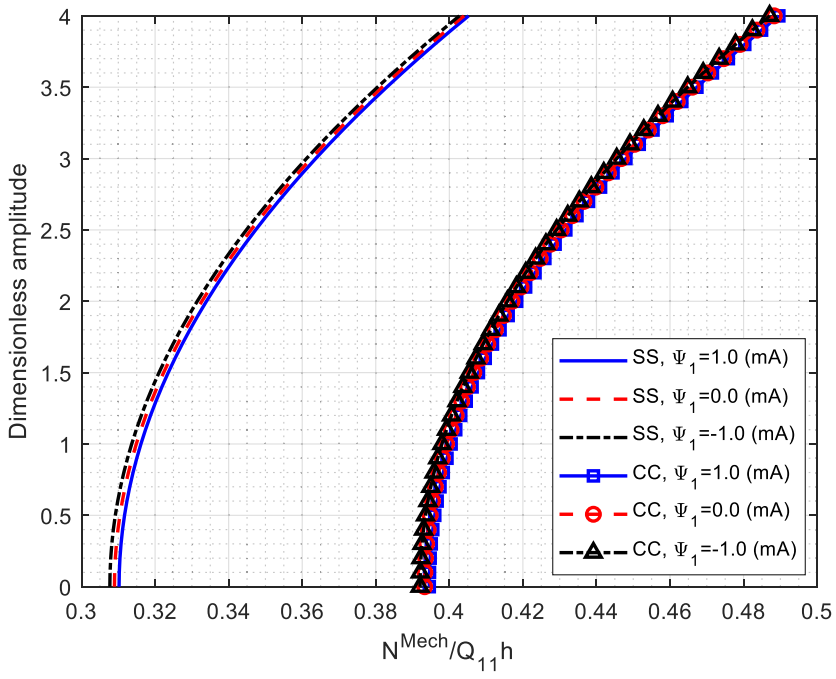

Fig. 8. Dimensionless amplitude versus dimensionless nonlinear buckling load in different applied external magnetic potentials.

due to an increase in dimensionless amplitude is more sensible in the case of SS end conditions than CC. The difference between linear and nonlinear buckling responses of ME nano-plate strips for both SS and CC boundary conditions becomes more by decreasing the slenderness ratio. Therefore, the effect of end conditions is not important at larger slenderness ratios.

5. Conclusions

Buckling and post-buckling analysis of shear deformable magneto-electric nano-plate strips considering the piezo-flexoelectric and piezo-flexomagnetic effects was developed in this paper in the framework of the NSG theory. The principle of minimum total potential energy was used to derive the differential governing equations and boundary conditions. Closed-form solutions for the nano-plate strip with simply supported and clamped ends were obtained so that accurate linear and nonlinear buckling loads were achieved. To show the accuracy of the proposed solution, several validations were presented. Numerical results were provided to show the effects of significant factors on stability performance. The presented closed-form solutions and numerical results are valuable for future analyses and the design of such nanostructures to prevent instability. The main conclusions can be expressed as follows:

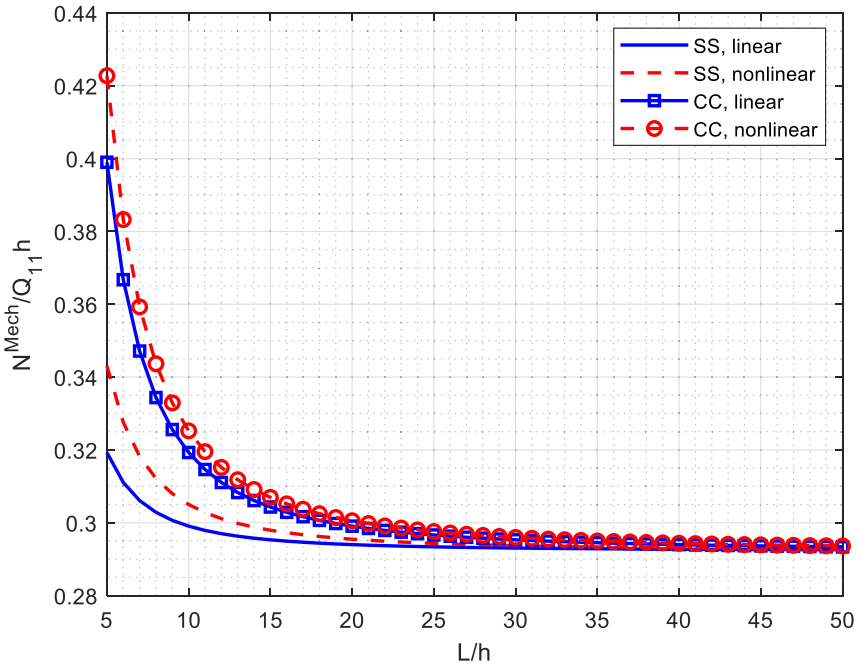

Fig. 9. Linear and nonlinear dimensionless buckling loads of the ME nano-plate strips with respect to the slenderness ratio for SS and CC end conditions.

- The post-buckling load-carrying capacity increases considerably in the case of a double-layer ME nano-plate strip compared to a single-layer (PFM or PFE) with the same thickness and length.
- The increase of initial magnetic potential leads to an increase of the electric resultant.
- The effect of applied electric voltage and magnetic potential on the buckling loads indicates that the highest stability is related to larger negative applied electric voltages and greater positive initial magnetic potentials. Hence, an appropriate selection of the external electric voltage and magnetic potential could improve the anti-buckling behavior of magnetoelectric nano-plate strips.
- The post-buckling deformation decreases with a decrease in initial electric voltage and an increase in initial magnetic potential.

CRediT authorship contribution statement

Hamed Momeni-Khabisi: Formal analysis, Methodology, Software, Validation, Writing – original draft. **Masoud Tahani:** Conceptualization, Project administration, Supervision, Writing – review & editing.

Declaration of competing interest

The authors declare that they have no known competing financial interests or personal relationships that could have appeared to influence the work reported in this paper.

Funding

This research did not receive any specific grant from funding agencies in the public, commercial, or not-for-profit sectors.

Data availability

Data will be made available on request.

Appendix A

The coefficients appearing in Eqs. (5) and (6) are defined as (Reddy, 2006; Sidhardh and Ray, 2018):

$$
\begin{aligned}
Q_{11} &= \frac{E}{1-\nu^2}, \quad Q_{12} = \nu Q_{11}, \quad C_{55} = \frac{Q_{11}(1-\nu)}{2} \\
g_{ijklmn} &= g_1\left[\left(\delta_{ij}\delta_{kl}+\delta_{ik}\delta_{jl}\right)\delta_{mn}+\left(\delta_{im}\delta_{ln}+\delta_{in}\delta_{lm}\right)\delta_{jk}\right] \\
&\quad + g_2\left[\left(\delta_{km}\delta_{ln}+\delta_{kn}\delta_{lm}\right)\delta_{ij}+\left(\delta_{jm}\delta_{ln}+\delta_{jn}\delta_{lm}\right)\delta_{ik}\right] \\
&\quad + g_3\delta_{il}\delta_{jk}\delta_{mn}+g_4\left(\delta_{jm}\delta_{kn}+\delta_{jn}\delta_{km}\right)\delta_{il} \\
&\quad + g_5\left[\left(\delta_{jn}\delta_{kl}+\delta_{jl}\delta_{kn}\right)\delta_{im}+\left(\delta_{jm}\delta_{kl}+\delta_{jl}\delta_{km}\right)\delta_{in}\right]
\end{aligned} \tag{A.1}
$$

with

$$
g_1 = -\frac{2}{3}\left(g_2+g_5\right), \quad g_2 = \frac{C_{55}}{30}\left(27l_0^2-4l_1^2-15l_2^2\right)
$$
$$
g_3 = \frac{8}{3}g_2+\frac{2}{3}g_5, \quad g_4 = \frac{C_{55}}{3}\left(l_1^2+6l_2^2\right), \quad g_5 = \frac{C_{55}}{3}\left(l_1^2-3l_2^2\right)
$$

where δ_{ij} is the Kronecker delta and l_0, l_1, and l_2 are material length scales.

Furthermore, the coefficients appearing in Eqs. (21)–(23) are defined as:

$$
\begin{aligned}
{}^p\lambda &= \sqrt{\frac{1+{}^pa_{33}\epsilon_0}{{}^pb_{33}\epsilon_0}}, \quad m_1(z) = \frac{{}^p\mu_{3113}}{\left(1+{}^pa_{33}\epsilon_0\right)}\left[\frac{e^{{}^p\lambda z}+e^{{}^p\lambda(z_1+z_0-z)}}{e^{{}^p\lambda z_1}+e^{{}^p\lambda z_0}}-1\right] \\
m_2 &= \frac{{}^p\mu_{3113}\left(z_1e^{{}^p\lambda z_1}-z_0e^{{}^p\lambda z_0}\right)}{\left(1+{}^pa_{33}\epsilon_0\right)\left(e^{2{}^p\lambda z_1}-e^{2{}^p\lambda z_0}\right)}+\frac{e_{31}{}^pb_{33}\epsilon_0}{\left(1+{}^pa_{33}\epsilon_0\right)^2\left(e^{{}^p\lambda z_1}+e^{{}^p\lambda z_0}\right)} \\
m_3 &= -\frac{{}^p\mu_{3113}e^{{}^p\lambda(z_1+z_0)}}{\left(1+{}^pa_{33}\epsilon_0\right)}\frac{z_1e^{{}^p\lambda z_0}-z_0e^{{}^p\lambda z_1}}{e^{2{}^p\lambda z_1}-e^{2{}^p\lambda z_0}}+\frac{e_{31}{}^pb_{33}\epsilon_0e^{{}^p\lambda(z_1+z_0)}}{\left(1+{}^pa_{33}\epsilon_0\right)^2\left(e^{{}^p\lambda z_1}+e^{{}^p\lambda z_0}\right)} \\
m_4 &= -\frac{{}^p\mu_{3113}}{\left(1+{}^pa_{33}\epsilon_0\right)}, \quad m_5 = -\frac{e_{31}}{\left(1+{}^pa_{33}\epsilon_0\right)} \\
m_6 &= -\frac{e_{31}{}^pb_{33}\epsilon_0}{\left(1+{}^pa_{33}\epsilon_0\right)^2}-\frac{e_{31}z_0z_1}{2\left(1+{}^pa_{33}\epsilon_0\right)} \\
m_7(z) &= \frac{\epsilon_0{}^p\mu_{3113}{}^p\lambda\left(e^{{}^p\lambda z}-e^{{}^p\lambda(z_1+z_0-z)}\right)}{\left(1+{}^pa_{33}\epsilon_0\right)\left(e^{{}^p\lambda z_1}+e^{{}^p\lambda z_0}\right)}-\frac{e_{31}}{{}^pa_{33}} \\
m_8 &= -\frac{2{}^p\mu_{3113}\epsilon_0{}^pa_{33}+{}^p\mu_{3113}}{{}^pa_{33}\left(1+{}^pa_{33}\epsilon_0\right)}-\frac{e31}{2{}^pa_{33}}\left(z_1+z_0\right)
\end{aligned} \tag{A.2}
$$

$$m_9(z) = \frac{\varepsilon_0 {}^p\mu_{3113} {}^p\lambda^2 \left(e^{{}^p\lambda z} + e^{{}^p\lambda(z_1+z_0-z)}\right)}{\left(1+{}^pa_{33}\varepsilon_0\right)\left(e^{{}^p\lambda z_1}+e^{{}^p\lambda z_0}\right)}$$
$$K_1(z) = \varepsilon_0 m_2 {}^p\lambda e^{{}^p\lambda z} - \varepsilon_0 m_3 {}^p\lambda e^{-{}^p\lambda z} + \varepsilon_0 m_5 z + m_8$$
$$K_2(z) = \varepsilon_0 m_2 {}^p\lambda^2 e^{{}^p\lambda z} + \varepsilon_0 m_3 {}^p\lambda^2 e^{-{}^p\lambda z} + \varepsilon_0 m_5$$

Appendix B

The stress resultants appearing in Eq. (8) are defined as:

$$\begin{aligned}&\left(N_{xx}, M_{xx}\right) = \int_{z_0}^{z_2} \sigma_{xx}\left(1, z\right) \mathrm{d}z \\ &Q_x = K_s \int_{z_0}^{z_2} \sigma_{xz} \mathrm{d}z, \quad N_{xxz} = \int_{z_0}^{z_2} \tau_{xxz} \mathrm{d}z\end{aligned} \tag{B.1}$$

The stress resultants in terms of displacement components are obtained as:

$$N_{xx} = D_1 \frac{\mathrm{d}u_0}{\mathrm{d}x} + D_2 \frac{\mathrm{d}\phi}{\mathrm{d}x} + \frac{1}{2} D_1 \left(\frac{\mathrm{d}w_0}{\mathrm{d}x}\right)^2 + D_3 \tag{B.2}$$

$$M_{xx} = D_4 \frac{\mathrm{d}u_0}{\mathrm{d}x} + D_5 \frac{\mathrm{d}\phi}{\mathrm{d}x} + \frac{1}{2} D_4 \left(\frac{\mathrm{d}w_0}{\mathrm{d}x}\right)^2 + D_6 \tag{B.3}$$

$$N_{xxz} = D_7 \frac{\mathrm{d}u_0}{\mathrm{d}x} + D_8 \frac{\mathrm{d}\phi}{\mathrm{d}x} + \frac{1}{2} D_7 \left(\frac{\mathrm{d}w_0}{\mathrm{d}x}\right)^2 + D_9 \tag{B.4}$$

$$Q_x = K_s A_{55} \left(\frac{\mathrm{d}w_0}{\mathrm{d}x} + \phi\right) \tag{B.5}$$

where D_i and A_{55} are given as follows:

$$\begin{aligned}
&D_i = {}^pD_i + {}^mD_i \qquad \text{for} \qquad (i = 1-9) \\
&{}^pD_1 = \int_{z_0}^{z_1} \left({}^pQ_{11} + e_{31}m_7 - {}^p\mu_{3113}m_9\right) \mathrm{d}z, \quad {}^mD_1 = \int_{z_1}^{z_2} {}^mQ_{11} \mathrm{d}z \\
&{}^pD_2 = \int_{z_0}^{z_1} \left({}^pQ_{11}z + e_{31}K_1 - {}^p\mu_{3113}K_2\right) \mathrm{d}z \\
&{}^mD_2 = \int_{z_1}^{z_2} \left[{}^mQ_{11}z + \frac{d_{31}^2}{2{}^ma_{33}}\left(2z - z_2 - z_1\right)\right] \mathrm{d}z \\
&{}^pD_3 = -\int_{z_0}^{z_1} \frac{e_{31}V_1}{{}^pa_{33}\left(z_1 - z_0\right)} \mathrm{d}z, \quad {}^mD_3 = \int_{z_1}^{z_2} \frac{d_{31}\Psi_1}{z_2 - z_1} \mathrm{d}z \\
&{}^pD_4 = \int_{z_0}^{z_1} \left({}^pQ_{11} + e_{31}m_7 - {}^p\mu_{3113}m_9\right) z \mathrm{d}z, \quad {}^mD_4 = \int_{z_1}^{z_2} {}^mQ_{11} z \mathrm{d}z \\
&{}^pD_5 = \int_{z_0}^{z_1} \left({}^pQ_{11}z + e_{31}K_1 - {}^p\mu_{3113}K_2\right) z \mathrm{d}z \\
&{}^mD_5 = \int_{z_1}^{z_2} \left[{}^mQ_{11}z + \frac{d_{31}^2}{2{}^ma_{33}}\left(2z - z_2 - z_1\right)\right] z \mathrm{d}z \\
&{}^pD_6 = -\int_{z_0}^{z_1} \frac{e_{31}V_1}{{}^pa_{33}\left(z_1 - z_0\right)} z \mathrm{d}z, \quad {}^mD_6 = \int_{z_1}^{z_2} \frac{d_{31}\Psi_1}{z_2 - z_1} z \mathrm{d}z \\
&{}^pD_7 = \int_{z_0}^{z_1} {}^p\mu_{3113}m_7 \mathrm{d}z, \quad {}^mD_7 = 0 \\
&{}^pD_8 = \int_{z_0}^{z_1} \left[{}^p\mu_{3113}K_1 + 2\left({}^p\alpha_2 + {}^p\alpha_4\right)\right] \mathrm{d}z \\
&{}^mD_8 = \int_{z_1}^{z_2} \left[{}^mg_{311311} + \frac{{}^m\mu_{3113}d_{31}}{2{}^ma_{33}}\left(2z - z_2 - z_1\right)\right] \mathrm{d}z \\
&{}^pD_9 = -\int_{z_0}^{z_1} \frac{{}^p\mu_{3113}V_1}{{}^pa_{33}\left(z_1 - z_0\right)} \mathrm{d}z, \quad {}^mD_9 = \int_{z_1}^{z_2} \frac{{}^m\mu_{3113}\Psi_1}{z_2 - z_1} \mathrm{d}z \\
&A_{55} = {}^pA_{55} + {}^mA_{55}, \quad {}^pA_{55} = \int_{z_0}^{z_1} {}^pC_{55} \mathrm{d}z, \quad {}^mA_{55} = \int_{z_1}^{z_2} {}^mC_{55} \mathrm{d}z
\end{aligned} \tag{B.6}$$

References

Amir, S., Khorasani, M., BabaAkbar-Zarei, H., 2020. Buckling analysis of nanocomposite sandwich plates with piezoelectric face sheets based on flexoelectricity and first-order shear deformation theory. J. Sandw. Struct. Mater. 22 (7), 2186–2209. http://dx.doi.org/10.1177/1099636218795385, arXiv:https://doi.org/10.1177/1099636218795385.

Ansari, R., Gholami, R., 2016. Nonlocal nonlinear first-order shear deformable beam model for postbuckling analysis of magneto-electro-thermo elastic nanobeams. Sci. Iran. 23 (6), 3099–3114. http://dx.doi.org/10.24200/sci.2016.4015, URL: http://scientiairanica.sharif.edu/article_4015.html.

Ansari, R., Gholami, R., 2017. Size-dependent buckling and postbuckling analyses of first-order shear deformable magneto-electro-thermo elastic nanoplates based on the nonlocal elasticity theory. Int. J. Struct. Stab. Dyn. 17 (01), 1750014. http://dx.doi.org/10.1142/S0219455417500146, arXiv:https://doi.org/10.1142/S0219455417500146.

Barati, M.R., Zenkour, A.M., 2019. Thermal post-buckling analysis of closed circuit flexoelectric nanobeams with surface effects and geometrical imperfection. Mech. Adv. Mater. Struct. 26 (17), 1482–1490. http://dx.doi.org/10.1080/15376494.2018.1432821, arXiv:https://doi.org/10.1080/15376494.2018.1432821.

Bibes, M., Barthélémy, A., 2008. Towards a magnetoelectric memory. Nature Mater. 7 (6), 425–426. http://dx.doi.org/10.1038/nmat2189.

Cheng, Y., Peng, B., Hu, Z., Zhou, Z., Liu, M., 2018. Recent development and status of magnetoelectric materials and devices. Phys. Lett. A 382 (41), 3018–3025. http://dx.doi.org/10.1016/j.physleta.2018.07.014, URL: https://www.sciencedirect.com/science/article/pii/S0375960118307394.

Duc, D.H., Thom, D.V., Cong, P.H., Minh, P.V., Nguyen, N.X., 2022. Vibration and static buckling behavior of variable thickness flexoelectric nanoplates. Mech. Based Des. Struct. Mach. 1–29. http://dx.doi.org/10.1080/15397734.2022.2088558, arXiv:https://doi.org/10.1080/15397734.2022.2088558.

Ebnali Samani, M.S., Tadi Beni, Y., 2018. Size dependent thermo-mechanical buckling of the flexoelectric nanobeam. Mater. Res. Express (Online) 5 (8), 18, URL: http://inis.iaea.org/search/search.aspx?orig_q=RN:51080598. NANOSCIENCE AND NANOTECHNOLOGY.

Ebrahimi, F., Barati, M.R., 2016a. Magneto-electro-elastic buckling analysis of nonlocal curved nanobeams. Eur. Phys. J. Plus 131 (9), 346. http://dx.doi.org/10.1140/epjp/i2016-16346-5.

Ebrahimi, F., Barati, M.R., 2016b. Static stability analysis of smart magneto-electro-elastic heterogeneous nanoplates embedded in an elastic medium based on a four-variable refined plate theory. Smart Mater. Struct. 25 (10), 105014. http://dx.doi.org/10.1088/0964-1726/25/10/105014.

Ebrahimi, F., Barati, M.R., 2018. Magnetic field effects on buckling characteristics of smart flexoelectrically actuated piezoelectric nanobeams based on nonlocal and surface elasticity theories. Microsyst. Technol. 24 (5), 2147–2157. http://dx.doi.org/10.1007/s00542-017-3652-x.

Ebrahimi, F., Karimiasl, M., 2018. Nonlocal and surface effects on the buckling behavior of flexoelectric sandwich nanobeams. Mech. Adv. Mater. Struct. 25 (11), 943–952. http://dx.doi.org/10.1080/15376494.2017.1329468, arXiv:https://doi.org/10.1080/15376494.2017.1329468.

Eliseev, E.A., Morozovska, A.N., Glinchuk, M.D., Blinc, R., 2009. Spontaneous flexoelectric/flexomagnetic effect in nanoferroics. Phys. Rev. B 79, 165433. http://dx.doi.org/10.1103/PhysRevB.79.165433, URL: https://link.aps.org/doi/10.1103/PhysRevB.79.165433.

Esmaeili, M., Tadi Beni, Y., 2019. Vibration and buckling analysis of functionally graded flexoelectric smart beam. J. Appl. Comput. Mech. 5 (5), 900–917. http://dx.doi.org/10.22055/jacm.2019.27857.1439, URL: https://jacm.scu.ac.ir/article_14245.html.

Ge, X., Ji, H., Li, Y., Chen, J., Wang, Y., 2018. Diameter and sequence effects on magnetoelectric effect in FeCo/Pb(Zr,Ti)O3/Ni trilayered long cylindrical composite structures. J. Alloys Compd. 752, 303–307. http://dx.doi.org/10.1016/j.jallcom.2018.04.153, URL: https://www.sciencedirect.com/science/article/pii/S0925838818314543.

Gunda, J.B., 2014. Thermal post-buckling and large amplitude free vibration analysis of Timoshenko beams: Simple closed-form solutions. Appl. Math. Model. 38 (17), 4548–4558. http://dx.doi.org/10.1016/j.apm.2014.02.019, URL: https://www.sciencedirect.com/science/article/pii/S0307904X14000766.

Gupta, R., Gunda, J.B., Ranga Janardhan, G., Venkateswara Rao, G., 2009. Comparative study of thermal post-buckling analysis of uniform slender and shear flexible columns using rigorous finite element and intuitive formulations. Int. J. Mech. Sci. 51 (3), 204–212. http://dx.doi.org/10.1016/j.ijmecsci.2009.01.002, URL: https://www.sciencedirect.com/science/article/pii/S0020740309000186.

Gupta, M., Meguid, S.A., Kundalwal, S.I., 2022. Synergistic effect of surface-flexoelectricity on electromechanical response of BN-based nanobeam. Int. J. Mech. Mater. Des. 18 (1), 3–19. http://dx.doi.org/10.1007/s10999-021-09582-6.

Kabychenkov, A.F., Lisovskii, F.V., 2019. Flexomagnetic and flexoantiferromagnetic effects in centrosymmetric antiferromagnetic materials. Tech. Phys. 64 (7), 980–983. http://dx.doi.org/10.1134/S1063784219070144.

Kambale, R.C., Kang, J.-E., Yoon, W.-H., Park, D.-S., Choi, J.-J., Ahn, C.-W., Kim, J.-W., Hahn, B.-D., Jeong, D.-Y., Kim, Y.-D., Dong, S., Ryu, J., 2014. Magneto-mechano-electric (MME) energy harvesting properties of piezoelectric macro-fiber composite/Ni magnetoelectric generator. Energy Harvest. Syst. 1 (1–2), 3–11. http://dx.doi.org/10.1515/ehs-2013-0026.

Kumaravel, A., Ganesan, N., Sethuraman, R., 2007. Buckling and vibration analysis of layered and multiphase magneto-electro-elastic beam under thermal environment. Multidiscip. Model. Mater. Struct. 3 (4), 461–476. http://dx.doi.org/10.1163/157361107782106401.

Kundalwal, S., Gupta, M., 2022. Interdependent effects of surface and flexoelectricity on the electromechanical behavior of BNRC nanoplate. Mech. Mater. 175, 104483. http://dx.doi.org/10.1016/j.mechmat.2022.104483, URL: https://www.sciencedirect.com/science/article/pii/S0167663622002472.

Kundalwal, S., Shingare, K., Gupta, M., 2020. Flexoelectric effect on electric potential in piezoelectric graphene-based composite nanowire: Analytical and numerical modelling. Eur. J. Mech. A Solids 84, 104050. http://dx.doi.org/10.1016/j.euromechsol.2020.104050, URL: https://www.sciencedirect.com/science/article/pii/S0997753820304381.

Li, Y., 2014. Buckling analysis of magnetoelectroelastic plate resting on Pasternak elastic foundation. Mech. Res. Commun. 56, 104–114. http://dx.doi.org/10.1016/j.mechrescom.2013.12.007, URL: https://www.sciencedirect.com/science/article/pii/S0093641313002085.

Li, L., Hu, Y., 2017. Post-buckling analysis of functionally graded nanobeams incorporating nonlocal stress and microstructure-dependent strain gradient effects. Int. J. Mech. Sci. 120, 159–170. http://dx.doi.org/10.1016/j.ijmecsci.2016.11.025, URL: https://www.sciencedirect.com/science/article/pii/S0020740316309134.

Li, P., Wen, Y., Bian, L., 2007. Enhanced magnetoelectric effects in composite of piezoelectric ceramics, rare-earth iron alloys, and ultrasonic horn. Appl. Phys. Lett. 90 (2), 022503. http://dx.doi.org/10.1063/1.2431469, arXiv:https://doi.org/10.1063/1.2431469.

Liang, X., Hu, S., Shen, S., 2015. Size-dependent buckling and vibration behaviors of piezoelectric nanostructures due to flexoelectricity. Smart Mater. Struct. 24 (10), 105012. http://dx.doi.org/10.1088/0964-1726/24/10/105012.

Lim, C., Zhang, G., Reddy, J., 2015. A higher-order nonlocal elasticity and strain gradient theory and its applications in wave propagation. J. Mech. Phys. Solids 78, 298–313. http://dx.doi.org/10.1016/j.jmps.2015.02.001, URL: https://www.sciencedirect.com/science/article/pii/S0022509615000320.

Majdoub, M.S., Sharma, P., Çağin, T., 2008. Dramatic enhancement in energy harvesting for a narrow range of dimensions in piezoelectric nanostructures. Phys. Rev. B 78, 121407. http://dx.doi.org/10.1103/PhysRevB.78.121407, URL: https://link.aps.org/doi/10.1103/PhysRevB.78.121407.

Malikan, M., Eremeyev, V.A., 2021a. Flexomagnetic response of buckled piezomagnetic composite nanoplates. Compos. Struct. 267, 113932. http://dx.doi.org/10.1016/j.compstruct.2021.113932, URL: https://www.sciencedirect.com/science/article/pii/S0263822321003925.

Malikan, M., Eremeyev, V.A., 2021b. Flexomagneticity in buckled shear deformable hard-magnetic soft structures. Contin. Mech. Thermodyn. http://dx.doi.org/10.1007/s00161-021-01034-y.

Malikan, M., Eremeyev, V.A., Żur, K.K., 2020a. Effect of axial porosities on flexomagnetic response of in-plane compressed piezomagnetic nanobeams. Symmetry 12 (12), http://dx.doi.org/10.3390/sym12121935, URL: https://www.mdpi.com/2073-8994/12/12/1935.

Malikan, M., Nguyen, V.B., 2018. Buckling analysis of piezo-magnetoelectric nanoplates in hygrothermal environment based on a novel one variable plate theory combining with higher-order nonlocal strain gradient theory. Phys. E 102, 8–28. http://dx.doi.org/10.1016/j.physe.2018.04.018, URL: https://www.sciencedirect.com/science/article/pii/S1386947717318131.

Malikan, M., Uglov, N.S., Eremeyev, V.A., 2020b. On instabilities and post-buckling of piezomagnetic and flexomagnetic nanostructures. Internat. J. Engrg. Sci. 157, 103395. http://dx.doi.org/10.1016/j.ijengsci.2020.103395, URL: https://www.sciencedirect.com/science/article/pii/S0020722520301828.

Malikan, M., Wiczenbach, T., Eremeyev, V.A., 2021. On thermal stability of piezo-flexomagnetic microbeams considering different temperature distributions. Contin. Mech. Thermodyn. 33 (4), 1281–1297. http://dx.doi.org/10.1007/s00161-021-00971-y.

Momeni-Khabisi, H., Tahani, M., 2022. A size-dependent study on buckling and post-buckling behavior of imperfect piezo-flexomagnetic nano-plate strips. Adv. Nano Res. 12 (4), 427–440. http://dx.doi.org/10.12989/ANR.2022.12.4.427.

Momeni-Khabisi, H., Tahani, M., 2023. Coupled thermal stability analysis of piezomagnetic nano-sensors and nano-actuators considering the flexomagnetic effect. Eur. J. Mech. A Solids 97, 104773. http://dx.doi.org/10.1016/j.euromechsol.2022.104773, URL: https://www.sciencedirect.com/science/article/pii/S0997753822002066.

Moradi-Dastjerdi, R., Meguid, S., Rashahmadi, S., 2019. Electro-dynamic analysis of smart nanoclay-reinforced plates with integrated piezoelectric layers. Appl. Math. Model. 75, 267–278. http://dx.doi.org/10.1016/j.apm.2019.05.033, URL: https://www.sciencedirect.com/science/article/pii/S0307904X19303300.

Pandey, R., Shankar, U., Meena, S.S., Singh, A.K., 2019. Stability of ferroelectric phases and magnetoelectric response in multiferroic (1-x)Bi(Ni1/2Ti1/2)O3-PbTiO3/xNi0.6Zn0.4Fe2O4 particulate composites. Ceram. Int. 45 (17, Part B), 23013–23021. http://dx.doi.org/10.1016/j.ceramint.2019.07.348, URL: https://www.sciencedirect.com/science/article/pii/S027288421932173X.

Reddy, J.N., 2006. Theory and Analysis of Elastic Plates and Shells, second ed. CRC Press, URL: https://doi.org/10.1201/9780849384165.

Ribeiro, C., Correia, V., Martins, P., Gama, F., Lanceros-Mendez, S., 2016. Proving the suitability of magnetoelectric stimuli for tissue engineering applications. Colloids Surfaces B 140, 430–436. http://dx.doi.org/10.1016/j.colsurfb.2015.12.055, URL: https://www.sciencedirect.com/science/article/pii/S0927776515304033.

Ryu, J., Kang, J.-E., Zhou, Y., Choi, S.-Y., Yoon, W.-H., Park, D.-S., Choi, J.-J., Hahn, B.-D., Ahn, C.-W., Kim, J.-W., Kim, Y.-D., Priya, S., Lee, S.Y., Jeong, S., Jeong, D.-Y., 2015. Ubiquitous magneto-mechano-electric generator. Energy Environ. Sci. 8, 2402–2408. http://dx.doi.org/10.1039/C5EE00414D.

She, G.-L., Yuan, F.-G., Ren, Y.-R., 2017. Thermal buckling and post-buckling analysis of functionally graded beams based on a general higher-order shear deformation theory. Appl. Math. Model. 47, 340–357. http://dx.doi.org/10.1016/j.apm.2017.03.014, URL: https://www.sciencedirect.com/science/article/pii/S0307904X17301634.

Shi, Y., Li, N., Ye, J., Ma, J., 2021. Enhanced magnetoelectric response in nanostructures due to flexoelectric and flexomagnetic effects. J. Magn. Magn. Mater. 521, 167523. http://dx.doi.org/10.1016/j.jmmm.2020.167523, URL: https://www.sciencedirect.com/science/article/pii/S0304885320324902.

Sidhardh, S., Ray, M.C., 2018. Flexomagnetic response of nanostructures. J. Appl. Phys. 124 (24), 244101. http://dx.doi.org/10.1063/1.5060672.

Yang, Y., Li, X.F., 2019. Bending and free vibration of a circular magnetoelectroelastic plate with surface effects. Int. J. Mech. Sci. 157–158, 858–871. http://dx.doi.org/10.1016/j.ijmecsci.2019.05.029, URL: https://www.sciencedirect.com/science/article/pii/S0020740319301924.

Yuan, S., Huang, Y., Zhou, J., Xu, Q., Song, C., Thompson, P., 2015. Magnetic field energy harvesting under overhead power lines. IEEE Trans. Power Electron. 30 (11), 6191–6202. http://dx.doi.org/10.1109/TPEL.2015.2436702.

Zhang, X., Chen, X., Li, M., Li, Y., Xu, J., 2021. Thermal post-buckling analyses of magneto-electro-elastic laminated beams via generalized differential quadrature method. Aerosp. Sci. Technol. 119, 107179. http://dx.doi.org/10.1016/j.ast.2021.107179, URL: https://www.sciencedirect.com/science/article/pii/S1270963821006891.

Zhang, E., Xu, L., Yu, G., Pan, F., Yang, K., 2009. In vivo evaluation of biodegradable magnesium alloy bone implant in the first 6 months implantation. J. Biomed. Mater. Res. Part A 90A (3), 882–893. http://dx.doi.org/10.1002/jbm.a.32132, URL: https://onlinelibrary.wiley.com/doi/abs/10.1002/jbm.a.32132, arXiv:https://onlinelibrary.wiley.com/doi/pdf/10.1002/jbm.a.32132.

Zhang, N., Zheng, S., Chen, D., 2019. Size-dependent static bending of flexomagnetic nanobeams. J. Appl. Phys. 126 (22), 223901. http://dx.doi.org/10.1063/1.5128940.

Zhang, N., Zheng, S., Chen, D., 2022a. Size-dependent static bending, free vibration and buckling analysis of curved flexomagnetic nanobeams. Meccanica 57 (7), 1505–1518. http://dx.doi.org/10.1007/s11012-022-01506-8.

Zhang, N., Zheng, S., Chen, D., 2022b. Size-dependent static bending, free vibration and buckling analysis of simply supported flexomagnetic nanoplates. J. Braz. Soc. Mech. Sci. Eng. 44 (6), 253. http://dx.doi.org/10.1007/s40430-022-03556-1.

Zhang, X., Zhou, J.-P., Yao, X., Yang, Z., Zhang, G.-B., 2020. Comprehensive analysis of direct and converse magnetoelectric effects in S-S mode bilayered composites. J. Magn. Magn. Mater. 501, 166411. http://dx.doi.org/10.1016/j.jmmm.2020.166411, URL: https://www.sciencedirect.com/science/article/pii/S0304885319332214.

Zhao, X., Zheng, S., Li, Z., 2022. Bending, free vibration and buckling analyses of AFG flexoelectric nanobeams based on the strain gradient theory. Mech. Adv. Mater. Struct. 29 (4), 548–563. http://dx.doi.org/10.1080/15376494.2020.1779880, arXiv:https://doi.org/10.1080/15376494.2020.1779880.

Zubko, P., Catalan, G., Tagantsev, A.K., 2013. Flexoelectric effect in solids. Annu. Rev. Mater. Res. 43 (1), 387–421. http://dx.doi.org/10.1146/annurev-matsci-071312-121634, arXiv:https://doi.org/10.1146/annurev-matsci-071312-121634.

Żur, K.K., Arefi, M., Kim, J., Reddy, J., 2020. Free vibration and buckling analyses of magneto-electro-elastic FGM nanoplates based on nonlocal modified higher-order sinusoidal shear deformation theory. Composites B 182, 107601. http://dx.doi.org/10.1016/j.compositesb.2019.107601, URL: https://www.sciencedirect.com/science/article/pii/S1359836819350310.